Segmentation of MRS signals using ASPECT (Analysis of SPectra using Eigenvector deComposition of Targets)

Joseph R. Roebuck[a)]
Bioengineering Program, University of Michigan, Ann Arbor, Michigan 48109

Joe P. Windham and David O. Hearshen
Department of Diagnostic Radiology, Henry Ford Hospital, Detroit, Michigan 48202

(Received 5 November 1992; accepted for publication 26 November 1993)

Efforts to minimize the effects of partial volume contamination (PVC) in *in vivo* magnetic resonance spectroscopy (MRS) have focused upon improving the sensitivity and efficiency of spatially localized MRS measurements. Such improvements may improve spatial resolution and reduce the time required to acquire multiple spectra, however, PVC can affect *in vivo* spectra at any resolution. In this paper, a model for segmenting *in vivo* MRS signals compromised by PVC in selected applications is introduced. The segmentation algorithm used is linear and is based on filters originally developed for image processing applications. The model is developed from first principles and evaluated using computer simulations. It is suited for segmenting multivoxel or chemical shift imaging data, and can be used with spectra acquired at any spatial resolution. It is used to estimate the size of the partial volumes contributing to a voxel compromised by PVC and the spatially selective signal components that would be expected to arise from these partial volumes if they could be measured directly. Several spectral perturbants present in *in vivo* MRS measurements violate the linearity assumptions underlying the model and produce systematic errors that must be accounted for. A number of perturbants are discussed, and the potential *in vivo* applications of the model are illustrated using solvent-suppressed ^{1}H–CSI spectra from the normal human brain.

Key words: nuclear magnetic resonance, partial volume contamination, segmentation, chemical shift imaging, human brain

I. INTRODUCTION

Magnetic resonance spectroscopy (MRS) has become an important tool for noninvasively studying the biochemistry of normal and pathological human tissues *in vivo*.[1–8] Despite this, *in vivo* MRS has yet to firmly establish itself as a clinical tool. Several factors are responsible for this, including the intrinsic insensitivity of MRS and the relative ability of various localization techniques to exclude unwanted signal contributions. These factors limit the spatial resolution and spatial selectivity of MRS and directly affect the qualitative and quantitative value of noninvasive measurements.[5,9,10] Inadequate spatial resolution and/or spatial selectivity effectively corrupts localized MRS signals by causing signal contributions from sources outside the volume of interest (VOI), to be included in the acquired signal. This effect is known as partial volume contamination (PVC) and can lead to incorrect conclusions concerning the identity and relative amounts of various biochemical species believed to arise from a specific tissue or lesion. As a result, subtle differences between normal and pathological tissues can be masked by PVC, especially in locations where the two tissue types mix with one another beyond the limits of MRS to resolve.

Efforts to minimize the effects of PVC have focused upon improving the sensitivity and efficiency of spatially localized MRS measurements. Several improvements have increased the relative sensitivity of single voxel MRS measurements, but signals must still be averaged over relatively large volumes of tissue to obtain an adequate signal-to-noise ratio (SNR) within a reasonable period of time.[9] Other improvements have increased the efficiency of acquiring multiple spatially localized spectra in a time efficient manner (e.g., chemical shift imaging),[11,12] but this does not necessarily translate into an improvement in spatial resolution. Furthermore, the acquisition of multiple spatially localized signals can exacerbate the problem, as several different signals can be compromised by PVC if special attention is not paid to voxel placement. Ultimately PVC can affect spatially localized signals at any spatial resolution, and the only way to eliminate the effects of PVC during signal acquisition is to prevent its occurrence by shaping each localized volume to conform to the local geometry of the VOI.[13]

In this paper, we introduce a model for segmenting MRS signals compromised by PVC in selected applications. The model described here incorporates a linear segmentation algorithm we term "ASPECT" (Analysis of SPectra using Eigenvector deComposition of Targets) that utilizes the properties of the eigenimage filter.[14] The model provides a closed-form solution to the segmentation problem and offers an operator-independent method for segmenting MRS spectra compromised by PVC. A functionally similar version of the model has been reported for volume determination in MRI,[15] however, a recent search of the literature indicates that no other post-processing methods have heretofore been implemented to correct the

 0094-2405/94/21(2)/277/9/$1.20

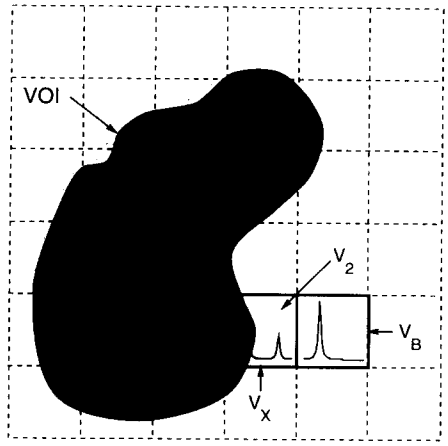

FIG. 1. The PVA model for two-component systems. The voxel V_X is composed of two partial volumes—one within the VOI and one outside the VOI. Given the spatial resolution of this measurement, the signals arising from the partial volumes cannot be measured directly, however, they can be estimated using the PVA model if the signal arising from V_X is modeled as a linear combination of the signals arising from V_A and V_B.

effects of PVC in spatially localized MRS. The model is developed from first principles and is based on the assumption that PVC can be modeled as a linear phenomenon. It is suited for segmenting multivoxel or chemical shift imaging (CSI) data, and can be used with spectra acquired at any spatial resolution. It is used to estimate the size of the partial volumes contributing to a voxel compromised by PVC and the spatially selective signal components that would be expected to arise from these partial volumes if they could be measured directly. The model and the ASPECT algorithm are fully developed for two-component systems—that is, for systems where PVC arises from only one undesired source—however, it is generally applicable and its extension to multicomponent systems is straightforward.

Violations of the assumption that PVC can be modeled as a linear phenomenon introduce systematic error into the analysis and restricts the potential utility of the model. Such violations are produced by biological heterogeneity and/or spectral perturbations, such as feature misregistration, phase differences, and differential saturation between spectra. The effects of these spectral perturbations on ASPECT is discussed and illustrated via simulation. The effect of biological heterogeneity is likely to be application specific, and must be characterized and/or corrected for in each case. As an example of its potential *in vivo* applications, the model is also demonstrated using solvent-suppressed ^{1}H–CSI spectra from a normal human brain.

A. The partial volume analysis model

Partial volume contamination results from incomplete superposition of a localized volume with the VOI. Figure 1 illustrates the spatial relationship that produces PVC from one undesired source. The VOI is shaded in the figure and the rectangular grid represents an array of contiguous voxels that intersect a plane through the VOI. Each voxel in the grid produces an extrinsic MRS signal that has contributions from all sources within it. Given the location and spatial resolution of these voxels, the signal arising from voxel V_X has contributions from partial volumes within the VOI and outside the VOI, and is thus compromised by PVC. The signal arising from voxels V_A and V_B are uncompromised in the sense that they are composed exclusively of contributions from sources within or outside the VOI. In a clinical scenario, this is analogous to V_X being composed of partial volumes of a lesion and contiguous normal tissue. In this case, the signal arising from V_X contains contributions from both and the unambiguous characterization of the tissue in V_X is compromised.

The partial volume analysis model for a two-component system seeks to segment the signal arising from V_X into the spatially selective signal components that arise from the partial volumes. To solve this problem, we model the signal arising from V_X as a linear combination of the signals arising from two other voxels. The use of a linear model requires that three assumptions be met. First, we assume the signal arising from V_X is composed of exactly two signal components, and that independent measurements of these signal components can be made. Second, we assume the signals arising from the two components are qualitatively different from one another and uniquely characterize their respective sources. Third, we assume that PVC is a linear phenomenon and the signals arising from a given source distribution are spatially invariant (i.e., the sample is homogeneously distributed across the voxel). While these assumptions limit the potential *in vivo* applications of the PVA model, they may not be unreasonable in certain applications. As an example, Fig. 1 illustrates the use of CSI to sample relatively small contiguous voxels that bracket the VOI. In this case, the assumptions may be reasonable, as the effects of biological heterogeneity are minimized given the proximity of the voxels and the simultaneous acquisition of all three input signals.

To model the partial volume problem, we define the spatially localized discrete time signal from V_X to be the target signal we wish to segment, and denote it $x[n]$. We assume that V_X is made up of contributions from two source distributions that are present in V_A and V_B. The discrete time signals from V_A and V_B are denoted $a[n]$ and $b[n]$, respectively. The signals $x[n]$, $a[n]$, and $b[n]$ are nominally N-point discrete time sequences derived from periodically sampling the corresponding free induction decays. Given the assumptions underlying the PVA model, $x[n]$ can be modeled as a linear combination of $a[n]$ and $b[n]$:

$$x[n]=\alpha a[n]+\beta b[n]. \tag{1}$$

If V_A, V_B, and V_X also denote their respective absolute volumes (in cm^3), then the partial volumes within the VOI and outside the VOI are $V_1=\alpha V_A$ and $V_2=\beta V_B$, respectively. The component signals arising from V_1 and V_2 are given by $x_A[n]=\alpha a[n]$ and $x_B[n]=\beta b[n]$, respectively. This analysis reduces the segmentation of $x[n]$ to acquiring the signals $a[n]$, $b[n]$, and $x[n]$, and solving (1) for α and β. We assume that the desired signals can be acquired using

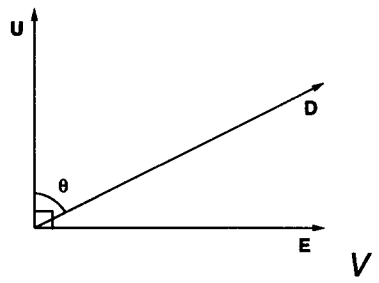

FIG. 2. The geometric relationship between **D**, **U**, and **E**. **D** and **U** are two linearly independent vectors that span the N-dimensional inner product space V, and θ is the angle between them. **E** is the vector in V that simultaneously maximizes the projection of **D** and suppresses the projection of **U** onto itself. The direction of **E** is given by Eq. (5).

various noninvasive spatial localization techniques. The solutions for α and β are estimated using the ASPECT algorithm described below.

B. The ASPECT algorithm

ASPECT is used to determine the values of α and β in (1) given the signals $x[n]$, $a[n]$, and $b[n]$. In theory, the N-point discrete time domain signals can be used directly, providing phase differences between the signals are eliminated. In practice, we generate the corresponding N-point discrete frequency domain signals $X[k]$, $A[k]$, and $B[k]$ and use only their pure absorption components. In the analysis that follows, these discrete sequences are denoted in terms of the N-dimensional vectors **X**, **A**, and **B**, and (1) is recast as the vector equation

$$\mathbf{X}=\alpha\mathbf{A}+\beta\mathbf{B}. \tag{4}$$

The ASPECT algorithm uses the properties of the eigenimage filter developed by Windham *et al.*[14] The eigenimage filter for two-component systems is developed from a contrast optimization criterion that seeks to maximize the projection of a desired feature, characterized by the vector **D**, while suppressing the projection of a single undesired feature, characterized by the vector **U**, onto an eigenvector **E**. Windham showed that there is only one nontrivial solution for **E**, and it is given by

$$\mathbf{E}=\mathbf{D}-\left(\frac{\mathbf{D}\cdot\mathbf{U}}{\mathbf{U}\cdot\mathbf{U}}\right)\mathbf{U}, \tag{5}$$

where $\mathbf{D}\cdot\mathbf{U}$ and $\mathbf{U}\cdot\mathbf{U}$ are scalar products. The geometric relationship between **D**, **U**, and **E** is illustrated in Fig. 2. There are four important properties of **E**, insofar as ASPECT is concerned: (a) **E** is always in the vector space spanned by **D** and **U**; (b) **E** always exists and $\mathbf{E}\neq\mathbf{0}$, except when $\mathbf{D}=k\mathbf{U}$; (c) the projection of **U** onto **E** is suppressed (i.e., $\mathbf{E}\cdot\mathbf{U}=0$); and (d) the projection of **D** onto **E** is not identically zero, except when $\mathbf{D}=k\mathbf{U}$. Note that **E** is the component of **D** orthogonal to **U** and can be derived using the Gram–Schmidt orthogonalization procedure.[16]

The properties of **E** are exploited by ASPECT to segment signals compromised by PVC into their individual components. To do this, we define the vector **X** to be the target vector we wish to segment, and the vectors **A** and **B** to be the constituents of **X**. The components **X** are then given by $\alpha\mathbf{A}$ and $\beta\mathbf{B}$, where α and β are termed the fractional components of **A** and **B** in **X**, respectively. In order to determine α and β, we form two eigenvectors, denoted $\mathbf{E}_A$ and $\mathbf{E}_B$, using (5). The geometric relationship between these eigenvectors and **A**, **B**, and **X** is illustrated in Fig. 3. The eigenvector $\mathbf{E}_A$ is formed by defining **A** as the desired feature and **B** as the undesired feature in (5):

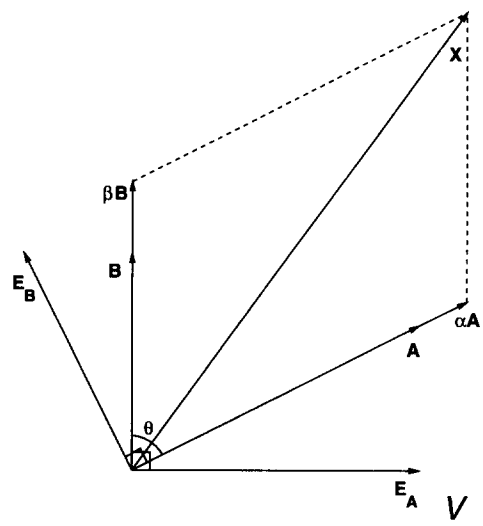

FIG. 3. The geometric relationship between **A**, **B**, **X**, $\mathbf{E}_A$, and $\mathbf{E}_B$. **A** and **B** are two linearly independent vectors that span V and θ is the angle between them. **X** is a linear combination of **A** and **B**. $\mathbf{E}_A$ is the vector in V that simultaneously maximizes the projection of **A** and suppresses the projection of **B** onto itself. $\mathbf{E}_B$ is the vector in V that simultaneously maximizes the projection of **B** and suppresses the projection of **A** onto itself.

$$\mathbf{E}_A=\mathbf{A}-\left(\frac{\mathbf{A}\cdot\mathbf{B}}{\mathbf{B}\cdot\mathbf{B}}\right)\mathbf{B}. \tag{6}$$

The eigenvector $\mathbf{E}_B$ is formed by reversing the assignments of **A** and **B** made above:

$$\mathbf{E}_B=\mathbf{B}-\left(\frac{\mathbf{B}\cdot\mathbf{A}}{\mathbf{A}\cdot\mathbf{A}}\right)\mathbf{A}. \tag{7}$$

Based on the eigenvector properties stated above, it follows that $\mathbf{E}_A\cdot\mathbf{B}=\mathbf{E}_B\cdot\mathbf{A}=0$. It also follows that $\mathbf{E}_A\cdot\mathbf{A}\neq 0$ and $\mathbf{E}_B\cdot\mathbf{B}\neq 0$, unless **A** and **B** are parallel.

In order to determine the fractional component of **A** in **X**, we form the scalar product $\mathbf{E}_A\cdot\mathbf{X}$ in (4) and solve for α:

$$\alpha=\frac{\mathbf{E}_A\cdot\mathbf{X}}{\mathbf{E}_A\cdot\mathbf{A}}. \tag{8}$$

Substituting (6) into (8), we obtain an expression for α in terms of **A**, **B**, and **X**:

$$\alpha=\frac{(\mathbf{A}\cdot\mathbf{X})(\mathbf{B}\cdot\mathbf{B})-(\mathbf{A}\cdot\mathbf{B})(\mathbf{B}\cdot\mathbf{X})}{(\mathbf{A}\cdot\mathbf{A})(\mathbf{B}\cdot\mathbf{B})-(\mathbf{A}\cdot\mathbf{B})^2}. \tag{9}$$

The expression for β is derived in analogous fashion and is given by

TABLE I. ASPECT segmentation of signals containing two features. Segmentation results are presented for two sets of data utilizing two well-resolved or two poorly resolved resonances. Rows 1A and 1B give segmentation results for deterministic data. SNR_A and SNR_B are the SNR values for the resonances in **A** and **B**, respectively. SNR_X^A and SNR_X^B are the SNR values of the resonances in **X** at the corresponding positions in **A** and **B**. α_e and β_e are the ASPECT estimates of α and β, where the predicted values (denoted α_p and β_p) are 2.00 and 5.00, respectively. $\Delta\%_\alpha$ and $\Delta\%_\beta$ are statistics used to compare the ASPECT estimates with the corresponding predicted values.

Two well-resolved resonances								
Row	S/N_A	S/N_B	S/N_X^A	S/N_X^{Ba}	α_e	$\Delta\%_\alpha$	β_e	$\Delta\%_\beta$
1A	...	...	...	...	2.000	...	5.000	...
2A	27.21	21.62	45.93	113.58	1.985	−0.75	4.942	−1.16
3A	13.28	10.61	23.09	56.08	1.928	−3.60	4.728	−5.44
4A	27.21	21.62	23.09	56.08	1.982	−0.75	4.940	−1.20
5A	13.28	10.61	45.93	113.58	1.931	−3.45	4.730	−5.40
Two poorly resolved resonances								
Row	S/N_A	S/N_B	S/N_X^{Ab}	S/N_X^{Bb}	α_e	$\Delta\%_\alpha$	β_e	$\Delta\%_\beta$
1B	...	...	...	...	2.000	...	5.000	...
2B	28.29	21.55	45.39	113.45	2.006	+0.30	4.934	−1.32
3B	14.41	10.57	22.77	56.90	2.035	+1.75	4.694	−6.12
4B	28.29	21.55	22.77	56.90	2.002	+0.10	4.933	−1.34
5B	14.41	10.57	45.39	113.45	2.038	+1.90	4.694	−6.12

[a]SNR_X values were calculated directly from **X**.
[b]SNR_X values were calculated indirectly from deterministic α_p**A** or β_p**B** and the noise signal added to deterministic **X**. This was required as a result of the degree of overlap of the features in **A** and **B**.

$$\beta=\frac{(\mathbf{B}\cdot\mathbf{X})(\mathbf{A}\cdot\mathbf{A})-(\mathbf{A}\cdot\mathbf{B})(\mathbf{A}\cdot\mathbf{X})}{(\mathbf{A}\cdot\mathbf{A})(\mathbf{B}\cdot\mathbf{B})-(\mathbf{A}\cdot\mathbf{B})^2}. \tag{10}$$

Note that the expressions for α and β are symmetric with respect to **A** and **B** and have identical denominators.

The PVA model and ASPECT algorithm are generally applicable to systems containing more than two components. In the case of multicomponent systems, (1) is expanded to include weighted contributions from several components and $x[n]$ is modeled as a linear combination of each. The corresponding vector equation for M components is given by

$$\mathbf{X}=\sum_{i=1}^{M}\alpha_i\mathbf{A}_i. \tag{11}$$

The values of each α_i are calculated from (8) using the corresponding generalized eigenimage filter, which can be computed directly using the Gram–Schmidt orthogonalization procedure.[17]

III. SIMULATIONS

Computer simulations were performed to test the accuracy of ASPECT and to illustrate the effects of varying random error, spectral resolution, and the complexity of its signal inputs when the linearity assumptions underlying the PVA model are satisfied. These results are summarized in Tables I and II and illustrated in Figs. 4–6. Additional simulations were performed to test the effects of violating the linearity assumptions underlying the PVA model by intentionally introducing systematic error in the form of various spectral perturbations. These results are summarized in Table III and illustrated in Figs. 7 and 8.

TABLE II. ASPECT segmentation of signals containing multiple overlapping features. Segmentation results are presented for a set of data that simulate *in vivo* ^{31}P-MRS spectra. Row 1 gives segmentation results for deterministic data. SNR values are given for the spectral feature corresponding to the PCr resonance. For rows 2–5, PCr has the highest SNR of the resonances present in each spectrum. The signals used here simulate *in vivo* ^{31}P-MRS spectra from a normal human brain (**A**), prolactinoma (**B**), and a mixture of the two (**X**). α_e and β_e are the ASPECT estimates of α and β, where the predicted values (denoted α_p and β_p) are 0.75 and 0.25, respectively. $\Delta\%_\alpha$ and $\Delta\%_\beta$ are statistics used to compare the ASPECT estimates with the corresponding predicted values.

Row	S/N_A	S/N_B	S/N_X	α_e	$\Delta\%_\alpha$	β_e	$\Delta\%_\beta$
1	...	...	...	0.750	...	0.250	...
2	29.35	22.26	27.51	0.746	−0.53	0.252	+0.80
3	14.51	11.66	13.80	0.726	−3.20	0.270	+8.00
4	29.35	22.26	13.80	0.747	−0.40	0.247	−1.20
5	14.51	11.66	27.51	0.726	−3.20	0.274	+9.60

All simulations were performed on a SUN 3/160 workstation equipped with a TAAC-1 application accelerator. Simulated data were created using the SA/GE™ spectral analysis software package (GE Medical Systems, Milwaukee, WI) and processed using an eigenanalysis program named SAGETOOL written in C. SAGETOOL inputs the signals **A**, **B**, and **X** and outputs estimates of the scalar constants α and β (denoted α_e and β_e) calculated by ASPECT

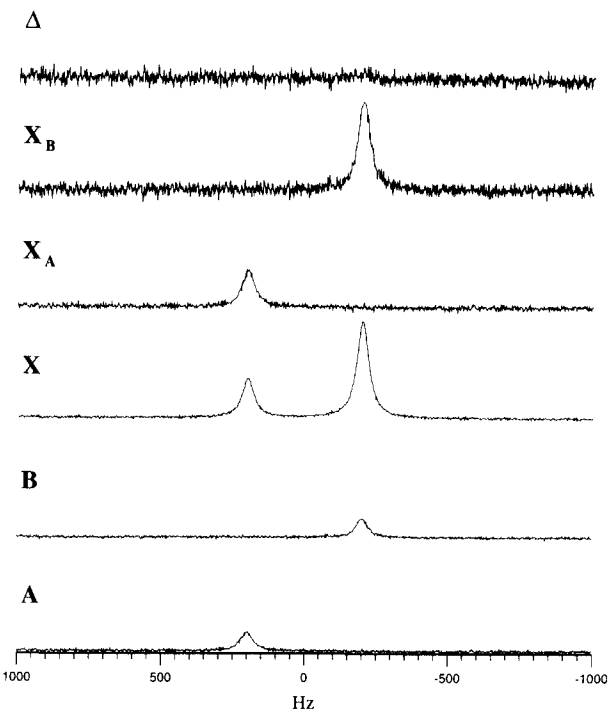

FIG. 4. ASPECT segmentation of two well-resolved features. **A** and **B** are simulated signals with added noise containing a single resonance with linewidth 50 Hz FWHM at 200 and −200 Hz, respectively. **X** is a simulated signal containing both resonances with $\alpha_p=2.000$ and $\beta_p=5.000$. Each signal consists of 1024 points and has a digital resolution of 0.5 points/Hz. $\Delta\%_\alpha$ and $\Delta\%_\beta$ are −3.60 and −5.44, respectively, and correspond to row 3A in Table I. Note that **Δ** has no remarkable features.

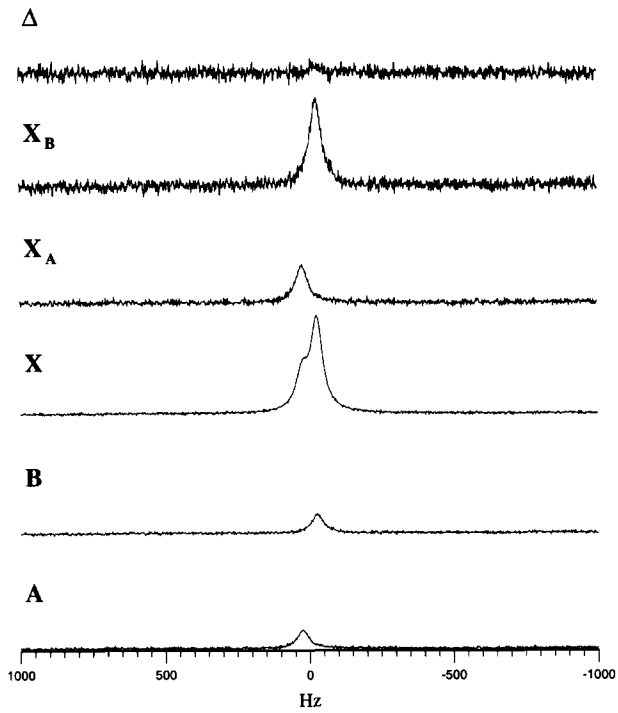

FIG. 5. ASPECT segmentation of two poorly resolved features. A and B are simulated signals with added noise containing a single resonance with linewidth 50 Hz FWHM at 25 and −25 Hz, respectively. X is a simulated signal containing both resonances with $\alpha_p=2.000$ and $\beta_p=5.000$. Each signal consists of 1024 points and has a digital resolution of 0.5 points/Hz. $\Delta\%_\alpha$ and $\Delta\%_\beta$ are +1.75 and −6.12, respectively, and correspond to row 3B in Table I. Note that Δ has no remarkable features.

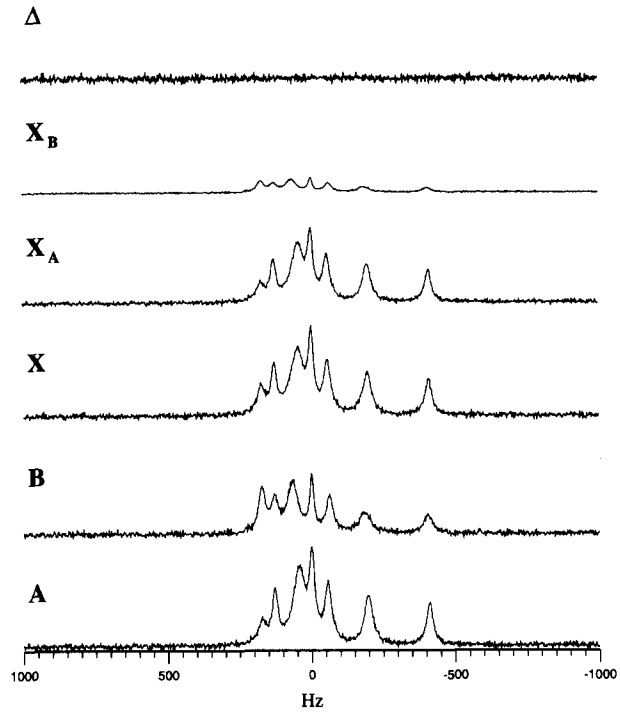

FIG. 6. ASPECT segmentation of multiple overlapping features. A and B are simulated ^{31}P–MRS spectra from a normal human brain and prolactinoma, respectively. X is a simulated signal containing contributions from both with $\alpha_p=0.75$ and $\beta_p=0.25$. In each signal, contributions are present from β, α, and γ resonances of ATP, PCr, PDE, P_i, and PME. Each signal consists of 1024 points and has a digital resolution of 0.5 points/Hz. $\Delta\%_\alpha$ and $\Delta\%_\beta$ are −0.53 and +0.80, respectively, and correspond to row 2 in Table II. Note that Δ has no remarkable features.

and the component signals α_e**A** and β_e**B**. The values of α_e and β_e are then compared to the predicted values of α and β (denoted α_p and β_p) and a statistic is calculated to compare the estimated and predicted values. This statistic is denoted $\Delta\%_\alpha$ or $\Delta\%_\beta$. In the case of α, $\Delta\%_\alpha$ is defined as the difference between α_e and α_p, and is expressed as a percentage of α_p. A significant $\Delta\%_\alpha$ value ($\geqslant$10%) indicates that the underlying cause (i.e., random or systematic error) has introduced a significant error component parallel or antiparallel to **A**, depending on the sign of $\Delta\%_\alpha$. $\Delta\%_\beta$ is similarly defined. This statistic is used to decipher general trends between simulations and small differences in $\Delta\%_\alpha$ or $\Delta\%_\beta$ may not be significant.

All signals within a given figure are identically scaled unless otherwise indicated. For those simulations incorporating added noise, the noise in the input signals is modeled after noise statistics observed in a set of ^{31}P–MRS experiments performed at 25.8 MHz. The noise in these signals was approximately normally distributed with a mean of zero and an average standard deviation of 6.51×10^8. Identical distributions were used to simulate uncorrelated noise spectra. Three different simulated noise spectra were then individually scaled and added to deterministic **X**, **A**, and **B** to produce input signals having uncorrelated random noise. The root mean square (RMS) of the noise for a given signal was varied by changing the scaling of the noise added to the deterministic signal. In each set of simulations, two simulations were performed in which **A**, **B**, and **X** have approximately equal RMS noise values. These simulations were done to simulate the noise characteristics expected in spatially localized MRS measurements from identically sized voxels, and are summarized in rows 2 and 3 in the tables. Two additional simulations were performed in which the relative levels of the RMS noise in **A** and **B** were smaller or larger than that present in **X**. These simulations were done to illustrate the effects of varying the

TABLE III. The effects of various spectral perturbations on ASPECT segmentation. Segmentation results for deterministic data that violate the linearity assumptions underlying the PVA model are presented. These segmentations use perturbed constituent signals (denoted **A′** and **B′**) and an unperturbed target signal evaluated from the expression $\mathbf{X}=\alpha_p\mathbf{A}+\beta_p\mathbf{B}$, with $\alpha_p=0.75$ and $\beta_p=0.25$. In row 1, the P_i resonance has been shifted by 25 Hz in **A′** and −25 Hz in **B′**. In row 2, the scale factors of **A** and **B** are reduced by 15% and 20% in **A′** and **B′** compared to their contributions in **X**. In row 3, time invariant (zeroth-order) phase shifts of 5° and −5° have been applied in **A′** and **B′**. In row 4, linear time varying (first-order) phase shifts of 30°/Hz and −30°/Hz have been applied in **A′** and **B′**.

Row	Perturbation	α_e	$\Delta\%_\alpha$	β_e	$\Delta\%_\beta$
1	Feature misregistration	0.690	−8.0	0.328	+31.2
2	Differential saturation	0.882	+17.6	0.312	+24.6
3	Zeroth-order phase	0.701	−6.5	0.336	+34.4
4	First-order phase	0.741	−1.2	0.242	−3.2

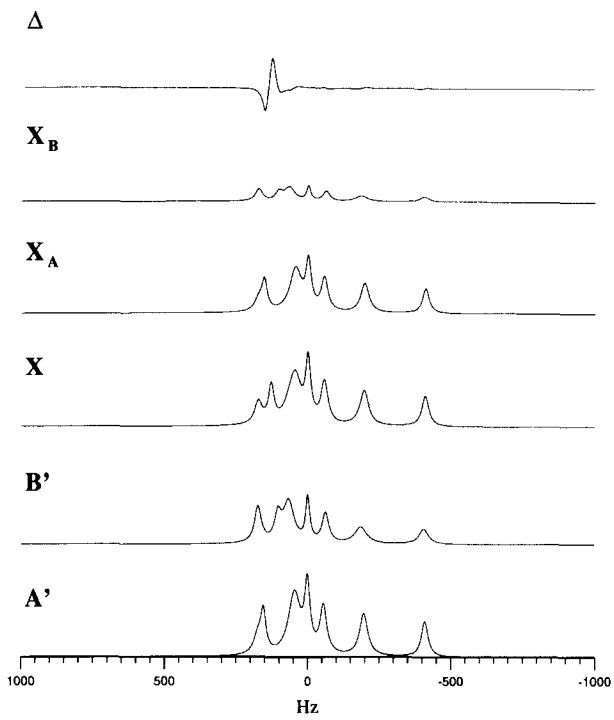

FIG. 7. The effects of feature misregistration on ASPECT. The P_i resonance has been misregistered in A' and B' compared to its location in X. This resonance is shifted by 25 Hz in A' and by −25 Hz in B'. $\Delta\%_\alpha$ and $\Delta\%_\beta$ are −8.0 and +31.2, respectively, indicating a significant parallel error component is present in X. Note the Δ has a large feature in the vicinity of the P_i resonance indicating a significant orthogonal component is also present in X.

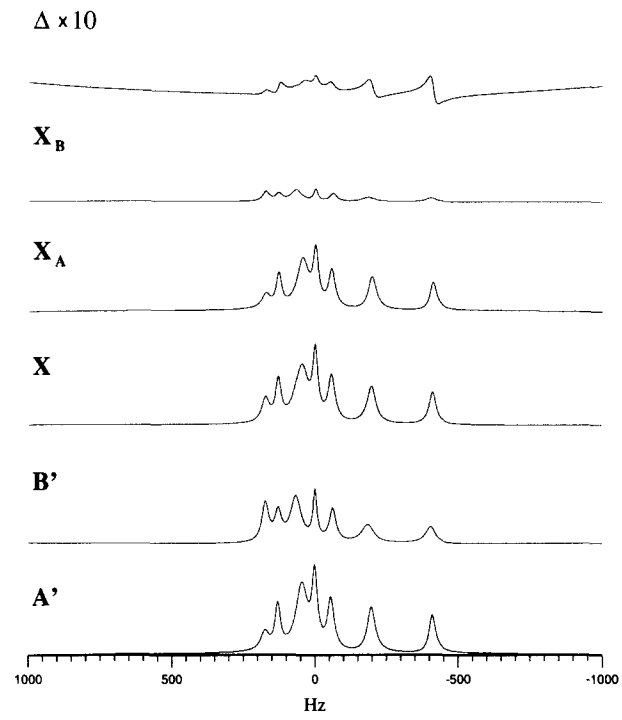

FIG. 8. The effects of time varying phase differences on ASPECT. A' and B' have small linear (first-order) phase differences compared to the in-phase contributions of A and B in X. A first-order phase shift of 30°/Hz has been applied to A and a shift of −30°/Hz has been applied to B to produce A' and B'. $\Delta\%_\alpha$ and $\Delta\%_\beta$ are −1.2 and −3.2, respectively, indicating that the parallel error components are insignificant. Note, however, that Δ is scaled×10 and has significant features across the range of resonances used, indicating a significant orthogonal component is present in X.

SNR in A and B versus varying the SNR of X, and are summarized in rows 4 and 5 in the tables.

In addition to the input signals, a number of other signals are shown in the figures. The components of A and B in X calculated using ASPECT (α_eA and β_eB) are denoted X_A and X_B, respectively. The residual signal, defined as $\Delta = X - (X_A + X_B)$, represents the component of X orthogonal to the vector space spanned by A and B. Thus, Δ is a qualitative measure of the accuracy of the segmentation. A Δ possessing significant features indicates that the linearity assumptions underlying the PVA model are invalid and that systematic error is likely to affect the segmentation. A Δ free of significant features indicates there are no orthogonal signal components resolved above the noise and is a marker that the signal components of X are parallel to A and B.

Table I shows the results of two sets of simulations intended to illustrate the effects of segmenting signals having only two features. These simulations were designed to test ASPECT using relatively simple signals. The first set used signals containing two well-resolved Lorentzian resonances (each resonance had a linewidth of 50 Hz FWHM and the two were separated by 400 Hz). The second set used signals containing two poorly resolved Lorentzian resonances (each resonance had a linewidth of 50 Hz FWHM and the two were separated by 50 Hz). In both sets, a deterministic segmentation and segmentations with varying amounts of added noise were performed. In each case, α_p and β_p were arbitrarily set to 2.000 and 5.000, respectively, and as such these simulations are not intended to model typical *in vivo* conditions. Rows 1A and 1B show that ASPECT is exact for deterministic data that satisfy the PVA model assumptions. This appears to be independent of the resolution of the spectral features. Table I also shows that ASPECT provides reasonable estimates of α_e and β_e with these data when added noise is present, as demonstrated by the relatively small Δ% values. Figures 4 and 5 demonstrate the segmentation results provided by ASPECT using noisy well-resolved and poorly resolved signals, respectively. In both cases, Δ has no significant features visible above the noise.

Table II shows the results of a set of simulations intended to illustrate the effects of segmenting signals having multiple overlapping resonances. These simulations were designed to test ASPECT with signals that simulate *in vivo* ^{31}P–MRS spectra. In this case, signals were simulated from published results.[18] These simulated signals were estimated by triangulation from spatially localized ^{31}P–MRS spectra of prolactinoma and uninfiltrated normal brain tissue. These signals contain resonances from adenosine triphosphate (ATP), phosphocreatine (PCr), phosphodiesters (PDE), inorganic phosphate (P_i), and phosphomonoesters (PME). The input signals in these simulations differ primarily in terms of the relative intensities of the

resonances present, however, there are also slight differences in the chemical shifts of several of these resonances. As in the previous segmentations, a deterministic segmentation and segmentations with varying amounts of added noise were performed. In these simulations, α_p and β_p were set to 0.75 and 0.25, respectively, in order to simulate the signals that may be acquired in a CSI experiment. In this case, V_X, V_A, and V_B are identically sized and V_X encompasses partial volumes of prolactinoma and normal tissue with normal tissue present as the larger partial volume. Table II shows that ASPECT is exact for deterministic signals containing multiple overlapping resonances and provides reasonable estimates of α_e and β_e with these data when added noise is present, as demonstrated by the relatively small $\Delta\%$ values. Figure 6 demonstrates the segmentation results provided by ASPECT using noisy simulated ^{31}P–MRS spectra. $\mathbf{\Delta}$ has no significant features visible above the noise.

While these simulations do not constitute an exhaustive study, a number of subtle characteristics are suggested by the data in Tables I and II. First, ASPECT's accuracy appears to be more sensitive to SNR_A and SNR_B than to SNR_X. This can be seen by first observing $\Delta\%$ values obtained when holding SNR_A and SNR_B constant and varying SNR_X and then observing the values obtained when holding SNR_X constant and varying SNR_A and SNR_B. In the former case the changes in $\Delta\%$ are relatively small, while in the latter case they are relatively large, with $\Delta\%$ values consistently decreasing as SNR_A and SNR_B are increased. Second, ASPECT's accuracy appears to be more sensitive to SNR_A and SNR_B than it is to the values of α_p and β_p. This can be seen by comparing $\Delta\%$ values in Tables I and II. In Table I, $\Delta\%_\alpha$ is consistently smaller than $\Delta\%_\beta$ for both well-resolved and poorly resolved signals, despite the fact that $\beta_p > \alpha_p$. This is because SNR_A is consistently larger than SNR_B which was an unanticipated result that arose from the location of the resonances in **A** and **B** and the randomness of the simulated noise spectra used. In Table II, $\Delta\%_\alpha$ is again consistently smaller than $\Delta\%_\beta$, however, in this case, $\alpha_p > \beta_p$. Finally, ASPECT's accuracy appears to be more sensitive to SNR_A and SNR_B than it is to the degree of overlap (and hence the vector direction) of **A** and **B**. This can be seen by comparing $\Delta\%$ values obtained for two poorly resolved resonances with those for two well-resolved resonances. In Table I, $\Delta\%_\alpha$ is consistently smaller, and $\Delta\%_\beta$ is consistently larger for poorly resolved signals than for the corresponding well-resolved signals. Note that the percent change between the two sets of simulations is greater for $\Delta\%_\alpha$ than it is for $\Delta\%_\beta$. This is because SNR_A is larger and SNR_B smaller for the poorly resolved signals than for the corresponding well-resolved signals, while SNR_X is approximately the same. Again, the relationship between SNR_A and SNR_B values arose from the location of the resonances in **A** and **B** and the randomness of the simulated noise spectra used.

Table III shows the results of a set of simulations intended to illustrate the effects of violating the linearity assumptions underlying the PVA model. These simulations were designed to test ASPECT with ^{31}P–MRS signals similar to those described above, with the exception that the spectral parameters (i.e., intensity, frequency, linewidth, and phase) were perturbed to produce a systematic error in the values of α_e and β_e. Such perturbations arise *in vivo* from a number of sample-dependent factors (e.g., biological heterogeneity, magnetic susceptibility gradients) and instrument-dependent factors (e.g., B_0 homogeneity, B_1 uniformity, and eddy currents). The size of the respective perturbations is somewhat exaggerated, in comparison to what may be encountered *in vivo*, and noise is absent in order to emphasize the magnitude of the systematic error.

Segmentations were performed using simulated signals perturbed by feature misregistration, differential saturation, and time invariant (zeroth-order) and linear time varying (first-order) phase differences between the features in the input signals. Significant $\Delta\%$ values ($>20\%$) are observed for feature misregistration, differential saturation, and zeroth-order phase differences, indicating significant parallel error components are present in **X**; smaller $\Delta\%$ values ($<5\%$) are observed for first-order phase differences. Examples of these segmentations are given for feature misregistration (Fig. 7) and linear time varying phase differences (Fig. 8). In each case, $\mathbf{\Delta}$ has features present, indicating an orthogonal signal component is present in **X**. This is most pronounced in Fig. 7, where a feature likely to be visible above ambient noise is present in the vicinity of the P_i resonance. Though not shown, a $\mathbf{\Delta}$ comparable to Fig. 8 was observed for zeroth-order phase differences, while the $\mathbf{\Delta}$ observed for differential saturation had no significant features. Collectively these results suggest that ASPECT is sensitive to these spectral perturbations and therefore the sample-dependent and instrumental factors that produce them. In addition, the segmentation modeling differential saturation confirms that $\mathbf{\Delta}$ is not a sensitive indicator for parallel error components unless a significant orthogonal error component is also present.

IV. DISCUSSION

A partial volume analysis model has been developed to segment MRS spectra compromised by partial volume contamination. The model is based upon linearity assumptions that limit the potential *in vivo* applications of the model, however, they may not be unreasonable in certain applications. The model uses an eigenanalysis based segmentation algorithm termed ASPECT that inputs the vector compromised by PVC and two vectors that characterize the partial volume components and outputs estimates of the fractional components of each signal component in the compromised spectrum.

Computer simulations utilizing two well-resolved resonances, two poorly resolved resonances, and simulated ^{31}P–MRS signals show that ASPECT is exact for deterministic data. This finding is independent of the number and resolution of the spectral features present. These data also show that ASPECT provides reasonable accuracy for well-resolved resonances ($\Delta\% \leqslant 5.4\%$), poorly resolved resonances ($\Delta\% \leqslant 6.2\%$), and simulated ^{31}P–MRS signals ($\Delta\% \leqslant 9.6\%$) when added noise is present. In addition, the simulations suggest that ASPECT's accuracy is more sen-

sitive to SNR_A and SNR_B than it is to SNR_X, the values of α_p and β_p, or the degree of overlap of **A** and **B**. The segmentation results demonstrate how the ASPECT estimates of α and β are used to decompose the target signal into its components. Notably, there are no remarkable features in the residual signals in these figures.

While ASPECT is easy to use and offers an operator-independent method for segmenting MRS spectra compromised by PVC, it is also sensitive to several sample and instrument-dependent factors expected to arise in *in vivo* measurements. These factors produce spectral perturbations that violate the linearity assumptions underlying the model. Several sources of error are identified and illustrated using computer simulations, including feature misregistration and phase differences between spectra. Significant $\Delta\%$ values ($>20\%$) are observed for feature misregistration and time invariant phase differences; smaller $\Delta\%$ values ($<5\%$) are observed for linear time varying phase differences. These error sources are present in *in vivo* data, where magnetic field inhomogeneity produce intervoxel frequency shifts and eddy currents produce time varying phase effects that typically manifest themselves as line shape distortions in the spectra. We have shown that the intervoxel frequency shifts and line shape distortions arising from eddy currents can be eliminated in CSI data without operator intervention by time domain phase correction using water reference spectra acquired under identical (or similar) conditions.[19] This correction has been applied to *in vivo* CSI data with good results (see below). The latter effect can also be eliminated in single voxel data by time domain phase correction, but intervoxel frequency shifts remain and must be corrected by other means. In both cases, the time invariant phase offset between the rotating frame and the absorption mode detector phase is also eliminated by the correction so no additional phasing is required to obtain pure absorption line shapes.

The effects of feature misregistration and phase differences between spectra highlight the need to perform carefully designed experiments and to correct for spectral perturbations that can be estimated on the basis of *a priori* information when using the PVA model with *in vivo* data. This leave differential saturation and biological heterogeneity as the main potential sources of systematic error. Both of these effects are minimized when using small volumes and contiguous volumes for **A**, **B**, and **X**. Preliminary work suggests that these conditions can be met *in vivo*. As an example, Fig. 9 illustrates an ASPECT segmentation of *in vivo* ^{1}H–CSI spectra taken from the occipital–parietal cortex in the human brain. **A**, **B**, and **X** are spectra taken from voxels containing predominantly gray matter (GM), white matter (WM), and a mixture of the two, respectively. The time domain phase correction has eliminated intervoxel frequency shifts and spectral asymmetries in the N-acetyl aspartate (NAA), creatine/phosphocreatine (Cr/PCr) and choline (Cho) resonances. The relative ratios of Cho/Cr and NAA/Cr in these spectra are consistent with literature values for GM and WM published by Kreis *et al.*,[20] suggesting that **A** and **B** accurately characterize the spectral features of GM and WM. The **Δ** produced shows no significant features, suggesting that ASPECT has accounted for the majority of the MRS signal present, despite the potential of biological heterogeneity and PVC to compromise the quality of **A** and **B**.

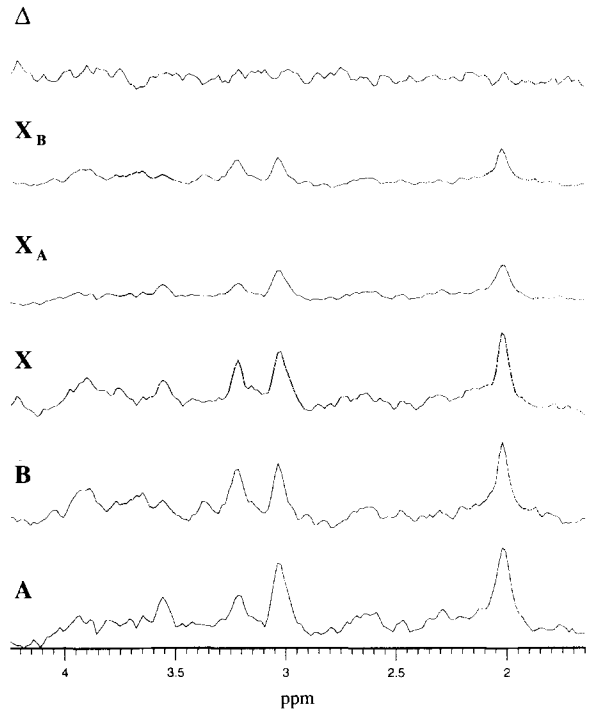

FIG. 9. ASPECT segmentation of ^{1}H–CSI spectra from a human brain. **A**, **B**, and **X** are STEAM spectra (TR 2000 ms, TE 30 ms, TM 11 ms, and 17 min acquisition time) taken from voxels containing GM (**A**), WM (**B**), and a mixture of the two (**X**), respectively. 1-D–CSI spectra are acquired by exciting a column of tissue (1.6 cm×1.6 cm×7.0 cm) localized across the midline in the occipital—parietal cortex and then phase encoding along the long axis of the column to produce an array of 1.6 cm×1.6 cm×0.4 cm CSI voxels. The CSI data are then corrected to eliminate phase and frequency offsets arising from eddy currents, B_0 inhomogeneity, and detector phase offsets. Signals from four CSI voxels (total volume 4.0 cm^3) containing either predominantly (>80%) GM, WM, or a mixture of the two are summed together and apodized using a 2.0 Hz exponential filter. The CSI voxels used for **X**, **A**, and **B** do not overlap, and the noise in the input signals is thus uncorrelated. Each signal consists of 1024 points with a digital resolution of 1.0 Hz/point. The points shown ($N=174$) defined the vectors used by ASPECT. α_e and β_e are 0.405 and 0.467, respectively. Note that **Δ** has no remarkable features visible above the noise in the vicinity of the Cho (3.2 ppm), Cr/PCr (3.0 ppm), and NAA (2.0 ppm) resonances.

The preliminary work presented here suggests the systematic errors encountered when using the PVA model with *in vivo* data may be overcome. Provided they are, the PVA model should improve the quality of *in vivo* spectra compromised by PVC. Ongoing work will focus on further characterizing the effects of random and systematic errors on ASPECT. In parallel with this, the PVA model will be tested using *in vitro* and *in vivo* MRS data to assess its applicability and range of use.

ACKNOWLEDGMENTS

The authors wish to thank Matt O'Donnell and Dave Reimann for helpful discussions. We also wish to thank Rita Bandhopadhyay, Steve Ramsey, and Lucie Bower for their assistance.

[a]To whom correspondence should be addressed at Division of MRI (WCB), Henry Ford Hospital, 2799 West Grand Blvd., Detroit, Michigan 48202.

[1]G. K. Radda, "The use of NMR spectroscopy for the understanding of disease," Science **233**, 640–645 (1986).

[2]M. W. Weiner, "NMR spectroscopy for clinical medicine. Animal models and clinical examples," Ann. NY Acad. Sci. **508**, 287–299 (1987).

[3]M. W. Weiner, H. Hetherington, B. Hubesch, G. Karczmar, B. Massie, A. Maudsley, D. J. Meyerhoff, D. Sappey-Marinier, S. Schaefer, D. B. Twieg, and G. B. Matson, "Clinical magnetic resonance spectroscopy of brain, heart, liver, kidney, and cancer. A quantitative approach," NMR Biomed. **2**, 290–297 (1989).

[4]J. D. Glickson, "Clinical NMR spectroscopy of tumors. Current status and future directions," Invest. Radiol. **24**, 1011–1016 (1989).

[5]P. A. Bottomley, "Human *in vivo* NMR spectrsocopy in diagnostic medicine: Clinical tool or research probe?," Radiology **170**, 1–15 (1989).

[6]P. F. Daly and J. S. Cohen, "Magnetic resonance spectroscopy of tumors and potential *in vivo* clinical applications: A review," Cancer Res. 49, 770–779 (1989).

[7]G. K. Radda, B. Rajagopalan, and D. J. Taylor, "Biochemistry *in vivo*: An appraisal of clinical magnetic resonance spectroscopy," Magn. Resonance Q. **5**, 122–151 (1989).

[8]W. Vine, "Clinical diagnosis by nuclear magnetic resonance spectroscopy. If not now, when?," Arch. Pathol. Lab. Med. **114**, 453–462 (1990).

[9]R. E. Lenkinski, "Clinical magnetic resonance spectroscopy: A critical evaluation," Invest. Radiol. **24**, 1034–1038 (1989).

[10]P. R. Luyten, J. P. Groen, J. W. Vermeulen, and J. A. den Hollander, "Experimental approaches to image localized human ^{31}P NMR spectroscopy," Magn. Resonance Med. **11**, 1–21 (1989).

[11]T. R. Brown, B. M. Kincaid, and K. Ugurbil, "NMR chemical shift imaging in three dimensions," Proc. Natl. Acad. Sci. USA **79**, 3523–3526 (1982).

[12]A. A. Maudsley, S. K. Hillal, W. H. Perman, and H. E. Simon, "Spatially resolved high resolution spectroscopy by 'four-dimensional' NMR," J. Magn. Resonance **51**, 147–152 (1983).

[13]J. C. Sharp and M. O. Leach, "Conformal NMR spectroscopy: Accurate localization to noncuboidal volumes with optimal SNR," Magn. Resonance Med. **11**, 376–388 (1989).

[14]J. P. Windham, M. A. Abd-Allah, D. A. Reimann, J. W. Froelich, and A. M. Haggar, "Eigenimage filtering in MR imaging," J. Comput. Assist. Tomogr. **12**, 1–9 (1988).

[15]D. J. Peck, J. P. Windham, H. Soltanian-Zadeh, and J. R. Roebuck, "A fast and accurate algorithm for volume determination in MRI," Med. Phys. **19**, 599–605 (1992).

[16]H. Anton, *Elementary Linear Algebra*, 2nd ed. (Wiley, New York, 1977), pp. 177–179.

[17]H. Soltanian-Zadeh and J. P. Windham, "Novel and general approaches to linear filter design for contrast-to-noise ratio enhancement of magnetic resonance images with multiple interfering features in the scene," J. Electron. Imag. **1**, 171–182 (1992).

[18]C. M. Segebarth, D. F. Baleriaux, D. L. Arnold, P. R. Luyten, and J. A. den Hollander, "MR image-guided P31 MR spectroscopy in the evaluation of brain tumor treatment," Radiology **165**, 215–219 (1987).

[19]J. R. Roebuck, D. O. Hearshen, M. O'Donnell, and T. E. Raidy, "Correction of phase effects produced by eddy currents in solvent suppressed ^{1}H-CSI," Magn. Resonance Med. **30**, 277–282 (1993).

[20]R. Kreis and B. D. Ross, "Cerebral metabolic disturbances in patients with subacute chronic diabetes mellitus: Detection with proton MR spectroscopy," Radiology **184**, 123–130 (1992).